APPLIED RESEARCH

Robust Target Classification Using UWB Sensing*

MAGDALENA BOUZA[1], **ANDRÉS ALTIERI**[1,2,3], **AND CECILIA G. GALARZA**[1,2]

[1]FIUBA, University of Buenos Aires (UBA), Buenos Aires 1063, Argentina
[2]Center for Computational Simulations (CSC), National Council for Scientific and Technological Research (CONICET), Buenos Aires 1425, Argentina
[3]Laboratoire des Signaux et Systèmes (UMR 8506), CentraleSupelec, CNRS, Université Paris-Saclay, 91190 Gif-sur-Yvette, France

Corresponding author: Magdalena Bouza (mbouza@fi.uba.ar)

ABSTRACT Contactless material characterization has received widespread attention in the radar and engineering domains. Specifically, impulsive Ultra Wideband (UWB) systems are a versatile technology for the nondestructive characterization of samples because the scattered field produced by the targets is highly dependent on their composition and shape. After the initial transient response to the transmitted pulse, the scattered signal can be decomposed as a sum of complex exponentials, called complex natural resonances (CNR), which are dependent only on the geometry and composition of the target. Using this result, a classification problem was formulated to discriminate among targets, and a processing strategy was proposed to solve it. In particular, by using spectral decomposition tools, the information obtained from the physical model can be exploited in combination with data-driven learning techniques. Consequently, a classification strategy that is robust to modeling uncertainties and experimental perturbations was designed. To assess the performance of the new scheme, it was tested using both synthetic and experimental data obtained from targets illuminated with a UWB radar. The results showed substantial gains compared to classification using time-domain signals.

INDEX TERMS Complex natural resonances, pattern classification, radar signal processing, spectral analysis.

I. INTRODUCTION AND MAIN CONTRIBUTIONS

The use of electromagnetic waves for noninvasive sensing has long been considered. Applications include radar and ground-penetrating radar (GPR) [1], [2], medical imaging [3], [4], disaster relief [5], bulk-material sensing [6], and through-the-wall imaging [7], [8]. An interesting application is the classification of targets according to their shape, position, or composition. In particular, contactless material characterization allows for nondestructive analysis of the composition of the device under test (DUT). This is a highly challenging problem because of the characteristics of the wireless medium; in general, specific solutions for each application and environment must be considered. In particular, Radiofrequency (RF) and Ultra Wideband (UWB) techniques, have gained relevance in this area [9], [10], [11], [12]. Specifically, impulsive UWB systems, which transmit

and receive pulses of very short duration, are a versatile technology for the nondestructive characterization of samples because the scattered field produced by a target is highly dependent on its composition and shape [13]. Impulsive UWB techniques have advantages in terms of low power consumption, flexible data rates, fine ranging, and high time resolution, compared to other UWB techniques such as Frequency-Modulation (FM) UWB [14]; therefore they have become prevalent in many applications. However, the approach discussed in this paper, is not exclusively limited to impulsive UWB systems.

In recent years, machine learning (ML) algorithms have gained increasing attention as a means of solving complex nonlinear tasks. It is expected that properly designed algorithms will be able to extract the necessary information from the input signals to attain a good performance in the task at hand. For example, ML has recently been explored as a natural candidate for solving wireless sensing problems [10], [12], [15], [16], [17]. In this context, the appropriate choice

The associate editor coordinating the review of this manuscript and approving it for publication was Hasan S. Mir.

of input features is critical and, in most cases, dictates the overall success of the learning strategy. Most solutions in the literature use standard feature extraction techniques that are not specifically tailored to wireless sensing and do not incorporate the benefits of an analytical model. For example, the authors in [11] investigated the performance of centimeter- and millimeter-wave radar units for material identification, with antennas in direct contact with the DUT. Eleven materials of different compositions were considered, all of which were set in containers of the same size. The extraction of features for both millimeter- and centimeter-wave radar antennas was performed by applying the wavelet scattering transform to raw time signals without considering a physical model.

Similarly, [12] proposed a Discrete Cosine Transform to extract the relevant features from 2D GPR simulations. However, this approach has not yet been validated using 3D experimental data. Other proposals, such as [15], classify targets using an array of transmitters and receivers to create a 2D image composed of raw electric field values that are processed using ML techniques. It is worth mentioning that this approach was also tested exclusively on synthetic data. Finally, [10] is an example in which the authors classify between different materials by considering certain physical properties. They generated a 2D image of the reflectance (amount of reflected power by a three-dimensional point) values of different materials and used ML image-processing techniques to classify the four different materials. The disadvantage of this technique is that it requires the sensor to be in contact with the DUT, which may be difficult in some scenarios. Although some of these studies have shown promising results, the proposed feature extraction and learning schemes do not generally exploit the domain knowledge of the signals. In addition, several approaches are solely data-driven and there is no indication of how they can be generalized to other types of scenarios.

In this paper, we address the problem of classifying targets of different compositions by incorporating the knowledge of a physical model in the feature extraction process. Specifically, we propose a model-based feature-building procedure that combines information from the analytical model with data-driven estimation techniques. For this purpose, we consider the fact that when a target is illuminated by an electromagnetic pulse, the transient scattered response is dominated by damped sinusoids that correspond to the complex natural resonances (CNRs) of the target [18], [19], [20]. In particular, CNRs depend only on the fundamental properties of the target such as material composition, electrical properties, size, and shape, making the set of CNRs a target signature. In this work, we introduce a novel preprocessing scheme for automatic feature extraction based on the CNRs, which are characteristic of each target.

Previous studies used CNRs to solve wireless classification problems. For example, in [21] and [22] the authors considered the classification of perfectly conducting (PEC) targets using CNRs. Although the authors obtained good results in

this case, the results were validated through simulations of targets in free space without perturbations. Furthermore, the CNRs for PEC targets are generally quite separated in the complex plane. In [23], the authors proposed a method for classifying conducting targets of simple shapes and different sizes using CNRs and ML techniques. The approach was validated through numerical simulations of PEC targets in free space in the presence of noise, obtaining good results in the high SNR regime. Reference [24] used CNRs to detect the presence of breast cancer. However, the simulation results were limited to comparing the plots of CNRs in a few specific scenarios. According to the authors, the work presented in [17] was the first to jointly use deep neural networks and CNRs to solve a target classification problem. The classification problem was solved using the first and second CNRs for different airplane scale models. More recently, in [25] the authors tested different ML algorithms to classify PEC targets with simple shapes by using CNRs for synthetic data. In [26] the author extended the application of the workflow to sphere targets of different compositions in addition to PEC. Again, this work was tested solely on simulated data, using both noiseless and noisy signals. Additionally, the permittivity values used to generate different materials are quite different from each other, with very few representing lossy materials.

The problem of estimating the CNRs is illposed in general, and is especially involved in the case of dielectric targets because in this case, the CNRs are typically very close to each other. Even when several high-resolution spectral estimation techniques are widely available, the accurate identification of damped resonances remains a challenge in practice. In addition, environmental perturbations and target variability make this problem even more challenging in real-world scenarios. For this reason, robust techniques are required.

The main contribution of this study is a general procedure for classifying dielectric targets according to their shape and composition in a non-invasive manner using scattered electromagnetic signals. The procedure, which is based on the CNRs of the targets, aims to be robust with respect to noise, measurement perturbations, and uncertainties owing to target construction variability. We tested our framework using both numerical examples and experimental measurements of dielectric targets. In the numerical examples, we analyzed the performance of the approach in a controlled setup under different perturbations. For the experimental setup, we considered the challenging problem of target classification based exclusively on composition. For this purpose, we observe objects of indistinguishable shapes composed of different materials. This makes for a more difficult problem since variations arising from shape differences are easier to detect than those produced by differences in composition [27]. In both cases, we compared the results with those obtained by processing time-domain signals. We demonstrate that the proposed approach yields a superior classification performance and robustness.

The remainder of this paper is organized as follows. In Section II, we introduce the signal model and address the classification problem. In doing so, we formulate the processing strategy that motivates this paper. In Section III we discuss some results to illustrate the performance of the proposed scheme. Finally, in Section IV, we elaborate on our concluding remarks.

II. CLASSIFICATION PROBLEM
A. PROBLEM STATEMENT

When a target is illuminated with an electromagnetic pulse, a scattered signal is generated. These scattered waves depend on various parameters such as the polarization of the incident pulse, incidence angle of the transmitted wave, observation angle, target material, size, and shape. In particular, if the wavelength of the incident pulse is of the order on the dimensions of the target, the scattering response can be modeled as the superposition of two signals: one due to direct reflections from the target, called the early time response, and another due to a resonance phenomenon, called the late time response [18]. The appeal of working with resonance phenomena lies in the fact that it is determined by the natural frequencies, which depend solely on the material composition, shape, and size of the target. In other words, these natural frequencies are independent of the aspect angle and polarization of the incident wave, and are unique for each object. A suitable model for static targets is the Singularity Expansion Method (SEM) [18], according to which the late time response, can be modeled as a sum of damped exponentials:

$$x(t) = \sum_{i=1}^{N} \alpha_i z_i^t, \quad t = 1, 2, \ldots, T, \quad (1)$$

where the scalars $z_i \in \mathbb{C}$ are the complex natural resonances (CNRs), also known as natural frequencies, and $\alpha_i \in \mathbb{C}$ are the complex residues. To account for the uncertainties in the experimental setup, we create a family of signals by taking into account variations in the residues., i.e.,

$$\mathcal{F}(z_1, \cdots, z_N) = \Big\{ x : \mathbb{N} \to \mathbb{C} : x(t) = \sum_{i=1}^{N} \alpha_i z_i^t,$$
$$\alpha_i \in \mathcal{B} \subset \mathbb{C}, i = 1, \cdots N \Big\}. \quad (2)$$

The family $\mathcal{F}$ is associated with a particular target, with a certain composition, shape, and form. The set $\mathcal{B}$ in which the residues lie, may be associated with different look angles for the target.

Suppose we have P families that satisfy (2), where the p-th family is characterized by N_p natural frequencies $z_{1,p}, \cdots, z_{N_p,p}$. To simplify the notation, we denote $\mathcal{F}_p(z_{1,p}, \cdots, z_{N_p,p})$ as $\mathcal{F}_p$. Although the number of classes is known, it is assumed that the number of natural frequencies N_p for each class and their resonances $z_{i,p}$ are unknown.

We define a noisy observation as

$$y(t) = x(t) + w(t), \quad t = 1, \cdots, T, \quad (3)$$

where $x(t)$ belongs to one of the $\mathcal{F}_p$ classes and $w(t)$ is a perturbation signal. We also define the vector

$$\mathbf{y} = [y(1), \ldots, y(T)] \in \mathbb{C}^T, \quad (4)$$

which corresponds to a finite record of noisy observations. A labeled set of observations $\{(\mathbf{y}^{(l)}, \rho^{(l)})\}_{l=1}^{L}$ is available to extract the relevant information that characterizes each class, where $\rho^{(l)} \in \{1, \cdots P\}$, and $\mathbf{y}^{(l)}$ correspond to noisy observation vectors same as in (4). The problem at hand can be summarized as follows:

Problem Statement: Given a finite set of labeled noisy observations $\{(\mathbf{y}^{(l)}, \rho^{(l)})\}_{l=1}^{L}$, where $\rho^{(l)} \in \{1, \cdots P\}$, design an algorithm to classify a new observation $\mathbf{y}$ into one of the P classes.

B. OVERVIEW OF THE PROPOSED SOLUTION

The proposed approach exploits the information provided by each z_i in (1) to classify signals. We consider the natural frequencies to be the distinctive elements of each class. As these elements are known only through training samples, a spectral estimation procedure must be employed. Many spectral estimation algorithms are tailored to line spectra and are robust against perturbations [28]. However, when N_p is unknown, different noisy vectors $\mathbf{y}_p$ from the same class p may lead to different sets of natural frequencies, possibly of variable sizes. A key element is to find an appropriate representation that simultaneously summarizes the spectral information of the observations and enables the comparison of different vectors among them. With the above problem in mind, we first outline the proposed solution, which we formalize in the next section. The main steps are as follows:

1) The number and values of the appropriate natural frequencies are estimated for each sample $\mathbf{y}^{(l)}$ in the training set. This step involves a spectral estimation procedure that returns a set of natural frequencies. In the end, L complex sets of possibly different sizes are obtained.

2) A mapping between each of the complex sets determined in the previous step and an M dimensional complex vector is defined. To obtain this vector, the complex plane is partitioned into M regions, each of which is associated with one component of the vector. For this purpose, the method considers the union of all sets of natural frequencies, and groups them into M sets using an appropriate clustering algorithm. This problem is not trivial, because it entails selecting a proper value for M and determining which natural frequency belongs to each region for each observation. It should be noted that the clustering procedure described does not perform signal classification. It only identifies regions of interest that contain a few natural frequencies from at least one sample in the training set. After determining M, the sets of natural frequencies obtained for each training signal are mapped onto their corresponding vectors in $\mathbb{C}^M$. Subsequently, the set of

training data is composed of L labeled M-dimensional complex vectors. A dimensionality reduction scheme is also implemented during the training session to retain only the most informative regions.

3) As the last step, a classifier is trained using the labeled M-dimensional vectors obtained in the previous step.

C. PREPROCESSING

The essence of our proposal is to pre-process the training data to obtain a suitable structure for the classification procedure. As a first step, each signal in the training set is processed individually to obtain its spectral information. For that, we resort to techniques based on subspace methods, as in [29]. In this section, we outline the procedure for a single signal in the training set. To simplify the notation, we drop the subindex indicating the class of the observation.

Let y be a noisy observation of $x(t) = \sum_{i=1}^{N} \alpha_i z_i^t$. The problem is to estimate N and the natural frequencies z_i, $i = 1, \cdots, N$. To cope with noise and uncertainties in N, we use optimization techniques that rely on Kronecker's theorem for Hankel operators. Let $\mathbf{H}(x) \in \mathbb{C}^{K \times N}$ represent the Hankel matrix constructed from the sampled signal $x(1), \cdots, x(T)$, where $T = K + N$. When N is known, Kronecker's theorem states that rank$(\mathbf{H}(x)) = N$. However, $x(t)$ is acquired only through noisy observations, $y(t)$. Then, a suitable denoising procedure is to solve the following optimization problem

$$\min_{\mathbf{A}, \tilde{y}} \quad \mathcal{I}_N(\mathbf{A}) + \sum_{j=1}^{K+N} |y(j) - \tilde{y}(j)|$$
$$\text{s.t.} \quad \mathbf{A} = \mathbf{H}(\tilde{y}), \tag{5}$$

where $\mathcal{I}_N(\mathbf{A})$ is a threshold function associated with the set $\{\mathbf{A} : \text{rank}(\mathbf{A}) \leq N\}$ [30]. Now using $\tilde{y}(t)$ we resort to a high-resolution spectral estimation technique, such as ESPRIT, to obtain the natural frequencies z_i, $i = 1, \cdots, N$.

Because N is unknown, model order selection techniques should be performed first, resulting in an estimation $\widehat{N}$. A sensible technique known as ESTER (ESTimation ERror) [31] computes an upper bound on the estimation error obtained with ESPRIT and selects the model order that minimizes such bound. A related approach, known as ubspace-based Automatic Model Order Selection (SAMOS), was introduced in [32]. However, it has been observed that both techniques exhibit a poor performance in noisy environments. On the other hand, using a hard threshold as in [33] to truncate the Hankel matrix $\mathbf{H}(y)$ tends to overestimate the model order when the SNR is high. In this work, we used a combined scheme, as presented in [34], in which a constrained optimization problem is posed with the function used in ESTER (or SAMOS).

The spectral estimation procedure transforms a noisy observation y into a set of estimated natural frequencies $\widehat{\mathbf{z}} = \{\hat{z}\}_{i=1}^{\widehat{N}}$, where $\widehat{N}$ is the estimated model order. The goal is to use the extracted sets of natural frequencies to compare different signals. However, natural frequencies are complex numbers that are not easily sorted, complicating the task of

pairing the natural frequencies to perform the comparison. An alternative is to map each complex natural frequency to a high-dimensional vector space and perform comparisons in this new space.

Let the union of all the sets of natural frequencies obtained for all the training vectors $\mathbf{y}^{(1)}, \ldots, \mathbf{y}^{(L)}$, be

$$\mathcal{Z} = \bigcup_{l=1}^{L} \widehat{\mathbf{z}}^{(l)} = \{\hat{z}_1^{(1)}, \ldots, \hat{z}_{\hat{N}^{(1)}}^{(1)}, \ldots, \hat{z}_1^{(L)}, \ldots, \hat{z}_{\hat{N}^{(L)}}^{(L)}\} \subset \mathbb{C}.$$

In general, the natural frequencies $\hat{z}_i^{(j)}$ for each target are concentrated in some regions in the complex plane. The goal is to identify these regions and use them to define a finite partition of the complex plane. For this purpose, we propose the application of a clustering procedure to $\mathcal{Z}$. In particular, we propose an agglomerative clustering scheme with complete linkage and Euclidean distance [35]. Complete linkage was chosen because it usually produces tighter clusters than other linkage methods, such as single-linkage. One benefit of Agglomerative Clustering is that it does not require previous knowledge of the number of clusters and does not make assumptions about the statistical properties of the data.

In the following, the procedure for creating clusters is described. Let c_i and c_j be two clusters. Due to the chosen metrics, the distance between two clusters is given by

$$d(c_i, c_j) = \max_{\hat{z}_l \in c_i, \ \hat{z}_m \in c_j} |\hat{z}_l - \hat{z}_m|. \tag{6}$$

The clustering procedure is iterative. For the first iteration, $k = 0$, each cluster is composed of one natural frequency. This results in a total of $Q = \sum_{i=1}^{L} \hat{N}^{(i)}$ clusters in the initial cluster set $\mathcal{C}_0$. At each subsequent step, the clusters with the minimum distance are merged together into a single cluster, and the cluster set is updated. Let $\mathcal{C}_{k-1}$ be the cluster set at the iteration $k - 1$. Then, $\mathcal{C}_k$ is obtained as follows:

$$\mathcal{C}_k = (\mathcal{C}_{k-1} \backslash c_1^k \backslash c_2^k) \cup c^{new}, \tag{7}$$

where $c_1^k, c_2^k = \arg\min_{c_i, c_j} d(c_i, c_j)$, $c^{new} = c_1^k \cup c_2^k$, and $\backslash$ is the set subtraction operator. This process is repeated until $d(c_i^k, c_j^k) > d_{th}$, for all i, j, where d_{th} is a previously selected threshold. By the end of the clustering process, there are $M \leq Q$ clusters. Each cluster is characterized by having CNRs which are at most at a distance of d_{th} from each other. These clusters define a partition of the complex plane. An important observation is that clustering is performed with the sole purpose of partitioning the complex plane to obtain some ordering of the CNRs.

As the last step in the presented preprocessing, we map the set of estimated natural frequencies of each individual sample, $\widehat{\mathbf{z}}^{(l)}$, $l = 1, \cdots L$, to a vector $\tilde{\mathbf{v}}^{(l)} \in \mathbb{C}^M$. To do so, we compute the k-th element of $\tilde{v}^{(l)}$ by averaging the elements of $\widehat{\mathbf{z}}^{(l)}$ found in the k-th region of the M-partition of $\mathbb{C}$. If there is no resonance in the k-th region for $\widehat{\mathbf{z}}^{(l)}$, then $\tilde{v}^{(l)}(k) = 0$. When we perform this operation on the training data, we map sets of varying cardinality, $\widehat{\mathbf{z}}^{(1)}, \cdots, \widehat{\mathbf{z}}^{(L)}$, into vectors that share the same space $\mathbb{C}^M$. The resulting vector $\tilde{\mathbf{v}}^{(l)} \in \mathbb{C}^M$
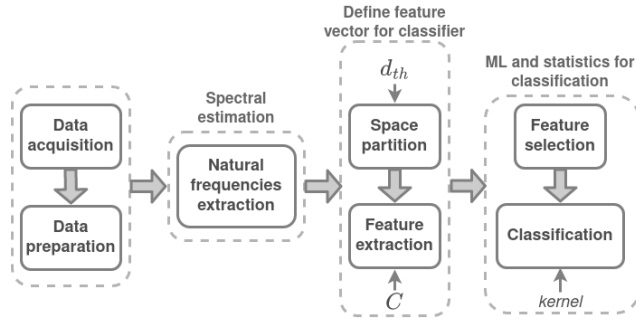
FIGURE 1. Data preprocessing and classification strategy, along with the hyperparameters to tune on each block.

defines the feature vector used as input in the classification step.

D. CLASSIFIER

As the result of the preprocessing of the training data, a set of features $\{\tilde{v}^{(l)}\}_{l=1}^{L}$ is obtained. Before training the classifier, a dimensionality reduction step is included. To select the most explicative features for the classification problem, we propose the use of a univariate test, namely the Kruskal-Wallis test. This non-parametric rank test examines whether all P classes have a common median [36]. If for a given feature the median is considered to be statistically the same for all classes, then it does not represent a useful feature for differentiating among said classes. The test assigns a number H_k to the k-th feature or dimension of vector $\tilde{v}$, indicating how informative this feature is. If the value of H_k is large, then the k-th feature contains discriminative information. We retain the $c\%$ more informative features, where c is a model hyperparameter. Finally, we obtain $v^{(l)} \in \mathbb{C}^d$, the reduced version of $\tilde{v}^{(l)} \in \mathbb{C}^M$. Here, d is the reduced number of features. The procedures described thus far result in the training set $\{(v^{(l)}, \rho^{(l)})\}_{l=1}^{L}$.

Using the training set $\{(v^{(l)}, \rho^{(l)})\}_{l=1}^{L}$, we train a P-ary classifier. The selected model is a Support Vector Machine (SVM) with a nonlinear kernel. The advantages of these classifiers are twofold: on the one hand, when using nonlinear kernels, they allow for nonlinear classification, and on the other hand, they perform well for small training sets, even when the number of samples is lower than the number of features. In addition, SVMs are robust to outliers and exhibit a good generalization performance [37]. SVMs are designed to operate on real inputs. Therefore, the inputs to the classifier are obtained by concatenating the real and imaginary parts of each $v^{(l)}$ in the training set.

Fig. 1 shows a block diagram of the classification strategy described previously. Each block shows the involved hyperparameters that must be selected for an optimal performance during the training process.

III. RESULTS

In this section, we describe the performance of the proposed classification strategy. We begin by analyzing synthetic data

designed to represent extreme scenarios that might arise in real-life applications. Afterward, we analyzes the results of the classification strategy applied to experimental measurements. In both cases, we compare the results obtained with the proposed method against the more traditional approach of using the time-domain signals y as input to the classifiers. For this approach, we train the SVM using the training set $\{(y^{(l)}, \rho^{(l)})\}_{l=1}^{L}$. Because we are dealing with complex signals, the input to this SVM is $[\Re\{y^{(l)}\}, \Im\{y^{(l)}\}]$, where $\Re\{y^{(l)}\}$ and $\Im\{y^{(l)}\}$ are the real and imaginary parts of $y^{(l)}$, respectively. In this case, the SVM input is $2T$-long. In the following, we shall refer to the proposed classification strategy based on natural frequencies as NF and the one processing the time-domain signals directly as TD.

To characterize the performance of each classification strategy, we considered two metrics computed over a set of S test samples, $\{(y^{(s)}, \rho^{(s)}), \rho^{(s)} = 1, \ldots, P\}_{s=1}^{S}$. When considering the s-th test sample, we say that $\rho^{(s)}$ is its true label, the actual class of the sample, and $\widehat{\rho^{(s)}}$ is the predicted one. One error metric is the error rate, which is the ratio of incorrectly classified instances to the total number of test samples

$$\varepsilon = \frac{\sum_{s=1}^{S} \mathbf{1}\{\widehat{\rho^{(s)}} \neq \rho^{(s)}\}}{S}.$$

A second metric is the confusion matrix, whose (i, j)-element represents the percentage of instances belonging to the i-the class that were classified as belonging to class j

$$\mathbf{E}_{ij} = \frac{\sum_{s=1}^{S} \mathbf{1}\{\widehat{\rho^{(s)}} = j, \rho^{(s)} = i\}}{\sum_{s=1}^{S} \mathbf{1}\{\rho^{(s)} = i\}} 100\%.$$

A. SYNTHETIC DATA

In this subsection, we discuss the performance of the proposed classification approach when applied to synthetic data. The goal is to validate the performance of the proposed classification scheme under challenging scenarios, in a controlled manner. The noiseless signals follow the model described in (1), and represent scattered signals from two different targets with similar shapes and compositions. Simulated signals correspond only to the late time response of the scattered signal since they are generated according to (1). In addition, it is worth mentioning that no clutter was considered at this stage. To assess the performance of the proposed technique, different perturbations are added to the baseline model.

For each class of signals as in (2), we generated several elements that were split to create the training and testing sets. In particular, we defined two families $\mathcal{F}_p$, $p = 1, 2$ whose nominal CNRs are $z_1 = \{0.1275 - 0.9075j, 0.44 - 0.16j, 0.97 + 0.02j, 0.57 + 0.79j, -0.19 + 0.94j\}$, and $z_2 = \{0.13 - 0.92j, 0.44 - 0.88j, 0.95 - 0.17j, 0.93 + 0.02j, 0.53 + 0.78j, -0.19 + 0.91j\}$ as shown in Fig 2. We set $T = 180$. These resonance values were selected to represent the challenging situation in which both classes are similar in both shape and composition. This is evidenced by the closeness between the CNRs of both classes. Additionally, in some
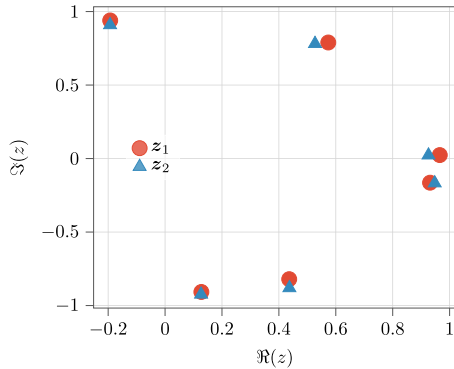
FIGURE 2. Complex natural resonances defining $\mathcal{F}_1$ and $\mathcal{F}_2$ used to generate synthetic data.

FIGURE 3. Training samples for each class of the synthetic example from Section III-A, when using SNR=10 dB, $\sigma_\alpha = 1$, and nominal CNRs.

TABLE 1. Performance of NF and TD classification when using nominal CNRs, SNR = 10 dB, and $\sigma_\alpha = 1$.

Strategy	ε	**E**		
			$\mathcal{F}_1$	$\mathcal{F}_2$
NF	0.073	$\mathcal{F}_1$	90.1%	9.9%
		$\mathcal{F}_2$	4.6%	95.4%
TD	0.331		$\mathcal{F}_1$	$\mathcal{F}_2$
		$\mathcal{F}_1$	60.4%	39.6%
		$\mathcal{F}_2$	26.5%	73.5%

FIGURE 4. Partition of the complex plane when using nominal CNRs, SNR=10 dB, and $\sigma_\alpha^2 = 1$. The Striped regions are those retained after feature selection. The Grey dots are the estimated CNRs, while the black crosses and triangles are the elements of sets z_1 and z_2 respectively.

simulations, we assume that the resonances are perturbed to represent situations in which there may be variability among different copies of identical targets.

The residues $\alpha_{i,p}$ for an element of $\mathcal{F}_p$, $p = 1, 2$, were obtained by independently sampling a complex Gaussian distribution with mean 0.5 and standard deviation σ_α. Each observation y is obtained by adding white noise sampled from a zero-mean circularly symmetric complex normal distribution with a variance σ_w^2. By varying σ_w^2, we changed the measured signal-to-noise ratio (SNR). We generated three different scenarios, each representing different levels of uncertainty in the model:

1) **Scenario 1, variable SNR:** We consider the nominal complex natural resonances and fix the uncertainty degree of the residues by considering a fixed value of σ_α^2. In particular, we considered $\sigma_\alpha^2 = 1$. We varied σ_w^2 to achieve different SNR values.

2) **Scenario 2, variable uncertainty in the residues:** Again, we consider the nominal CNRs, but now we select σ_w^2 to achieve an SNR=10dB. We varied the sets B_p by sampling from distributions with increasing variance σ_α^2.

3) **Scenario 3, uncertainties in the CNRs:** In this scenario, we analyze the uncertainties on the natural frequencies. For this, we fixed σ_w^2 and σ_α^2, and added perturbations to the natural resonances, which were generated from a complex circularly symmetric normal distribution with zero-mean and variance σ_z^2. We used $\sigma_\alpha = 1$, and σ_w^2 was selected such that the SNR was 10 dB.

For each scenario and each value of $(\sigma_\alpha, \text{SNR}, \sigma_z)$, we created three sets of signals for each family for training, while considering 1000 different sets for testing. This shows the robustness of the proposed method for low sample training. Fig. 3 shows $|y^{(k)}|$ when SNR=10dB, $\sigma_\alpha^2 = 1$ and the natural frequencies in z_1 and z_2 are unperturbed. Note that variations among the same family are comparable to variations between families.

First, we analyzed the preprocessing procedure when nominal CNRs were used for each class. Fig. 4 depicts the
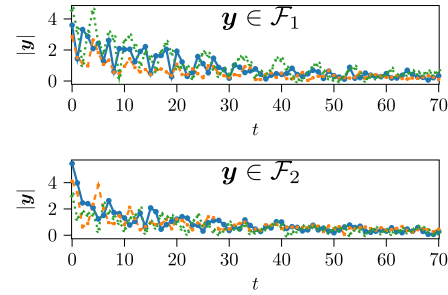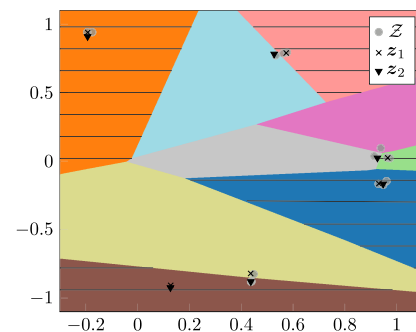
estimated and true resonances in the training set along with the partition in M regions obtained for the complex plane. In this case, the threshold for the clustering algorithm was $d_{th} = 0.03$, which was the optimal value obtained via cross-validation. Using this threshold, we obtained a partition of $M = 9$ regions. After performing feature selection, we retained the regions associated with the most representative features, which are shown as striped regions in Fig. 4. We were able to reduce the number of training features by almost half. This demonstrates a significant reduction in the number of inputs to the classifier: whereas the NF strategy requires only five regions (10 features) to train the SVM, the corresponding time signal consists of $T = 180$ points (360 features).

Table 1 lists the errors and confusion matrices of both strategies for the same scenario. As anticipated, the time-domain approach shows poor performance because it cannot differentiate between variations within the same
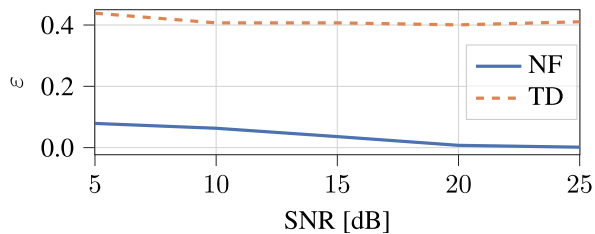
FIGURE 5. Classification error for Scenario 1.

FIGURE 6. Classification error for Scenario 2.

FIGURE 7. Classification error for Scenario 3.

family from those arising among classes. Figure 5 shows the error obtained for Scenario 1 for different SNR values [dB] for both NF and TD strategies. We observed that for all tested SNR levels, the classification performance based on natural frequencies was significantly better than that based on time-domain signals. Additionally, we observed a significant improvement as the SNR increased for the NF classifier, which did not occur under the TD approach. The TD strategy relies strongly on the values of the residues associated with each natural frequency in model (2). Variations in residues, which are associated to experimental conditions such as incidence angle and polarization of the incident pulse, lead to sensible disparities in the time-domain signals within the same family, as shown in Fig. 3. Consequently, the classifier presents poor performance when separating families. This is why an increase in the SNR did not significantly decrease the error. However, by extracting the natural frequencies, the NF strategy became independent of the residues. Moreover, an increase in the SNR resulted in a more accurate estimation of the resonances, thereby improving the classifier error.

Fig. 6 presents the results achieved for Scenario 2. Here, the sets show variations in B_p, obtained by sequentially increasing the variance of the distribution from which the residues were sampled. For a sufficiently low variance, both classifiers attain zero error. When the sets B_p are small, the residues associated with one natural frequency are quite similar among different realizations of the signals y, making all time-domain signals from the same class very close to each other. By eliminating the variations associated with the residues, even the TD approach achieved no classification error on the test set when SNR=10 dB. As σ_α^2 increases, signals from the same family begin to differentiate more from one another, thereby affecting the classification performance. However, one can see that these variations had a much greater impact on the TD strategy than on the NF strategy. While the TD strategy's performance deteriorates significantly, the classification error in the NF strategy remains below 0.1, even for large values of σ_α.

Finally, Fig. 7 compares the performance of both classifiers under Scenario 3. As σ_z^2 increased, so did the variability of the CNRs among the measurements of the same class. In this case, the performance of both classifiers decreased as the perturbations increased. This is expected because nominal CNRs from both families were purposely chosen to be close to each other, and as σ_z^2 increases, there is a greater chance of
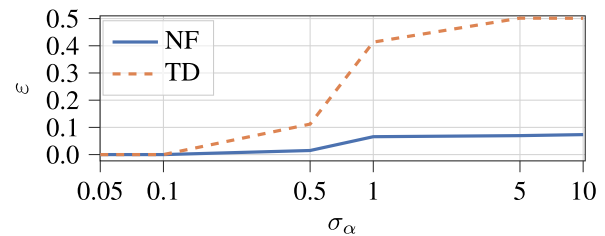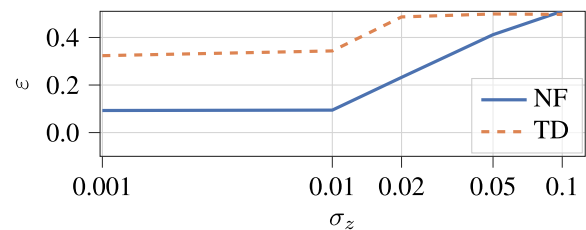
confusion between families. However, for values of σ_z below 0.1, the proposed method presents a significant improvement with respect to the TD classifier. The rapid increase in the error was a result of the overlapping resonance regions. The minimum and maximum distances between frequencies were 0.016 and 0.06, respectively. This explains why we observed a decline in performance when the uncertainty σ_z exceeded 0.01. At this uncertainty level, some of the natural frequencies of the two classes overlap for certain realizations. Moreover, when σ_z was larger than 0.1, overlapping occurred with a high probability for all natural resonances. Consequently, the scheme loses its prediction ability, and the observed error converges to the error when randomly choosing a class for each signal.

B. EXPERIMENTAL MEASUREMENTS

In this subsection, we test the performance of the proposed approach when dealing with experimental data. For this, we considered the scattering from a target illuminated with microwave signals in an experiment similar to that in [38]. The aim of the experiment was to classify targets that had the same shape and size, but different material compositions. Each target was illuminated by a UWB electromagnetic pulse, and the resulting scattering signal was collected by the receiving antenna.

For the proposed experiment, we considered a classification problem among plastic bottles containing three different liquids: alcohol (98%), tap water, and brine, with the latter being obtained by diluting 35 g of salt in 500 ml of water. The liquids were poured into identical containers, each of 500 ml of volume, in order to create targets with the same shape, weight, and color because all the liquids were transparent. Therefore, the only difference was the composition of the liquids making traditional approaches based on a target image or weight ineffective. All measurements were carried out

in a stationary environment, where all clutter behavior is predictable and repeatable, similar to a lab environment or a dedicated device for target classification. For this reason, we chose to omit clutter reduction techniques at this stage. Several studies have been conducted in this manner [17], [39].

We used the X4M06 Radar Development Kit, which is based on the XeThru X4 UWB system-on-chip developed by Novelda [40]. This platform emits pulses with a bandwidth of 1.5 GHz at a central frequency $f_c = 8.748$ GHz, and receives the scattered response. The power transmission of this device is within the limits set by the FCC. The captured pass-band response is sampled by the system at an equivalent-time sampling frequency of $f_s = 23.328$ GS/s and downconverted in the PC to obtain the complex baseband equivalent signal. To improve the signal-to-noise ratio, the platform transmits numerous pulses and averages the scattered response over multiple transmissions to mitigate random interference and noise. The decision to use the X4M06 radar was based mostly on availability and cost. While this system is based on impulse radio UWB technologies, the presented work could be used for measurements taken with other UWB sensors, although more preprocessing of the raw signals might be required.

We performed several measurements of the scattered response on each target to diversify the training set. An image of the experimental setup can be found in 8. The targets were located at nine positions, and scattered signals from each target were collected for each position. For this purpose, we located the targets along a line parallel to the antennas, at a distance of 40cm. Along this line, we chose nine different points, each separated by 5 cm. In addition, we oriented each target vertically and horizontally (Fig. 9). For each position and orientation, we took 10 measurements of the scattered response. The signal returned by the XeThru, which has a fixed length of $T = 1497$ samples, is denoted by $s(t)$. This scattered signal can be decomposed as:

$$s(t) = x(t) + w(t) + d(t), \quad t = 1, \ldots, T, \quad (8)$$

where $x(t)$ is the true scattered response, $w(t)$ is the noise and radio frequency interference from the environment, and $d(t)$ is due to antenna cross-coupling and clutter in general. Assuming that the noise and interference in $w(t)$ are stationary for the duration of transmissions, they are mitigated by the internal averaging process performed by transceiver module. However, the disturbance $d(t)$ is persistent and is not mitigated by averaging. Moreover, this disturbance does not have a linear interaction with the scattered response of the target. However, one could take an additional measurement with no target present and extract its natural frequencies, which would be associated with reflections from objects in the background. These resonances are also present in the scattering measured from each target, and most of them are discarded in the feature selection stage, as shown in Fig. 11.

Fig. 10 shows the signals received by the XeThru for each target located at 40 cm of the antennas and vertically aligned. This figure depicts the antenna coupling signal,
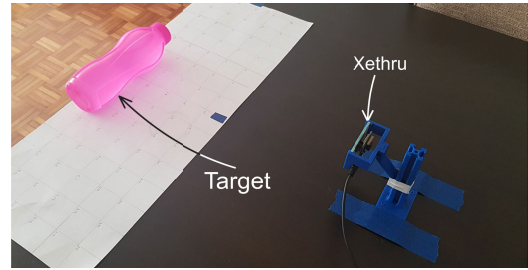

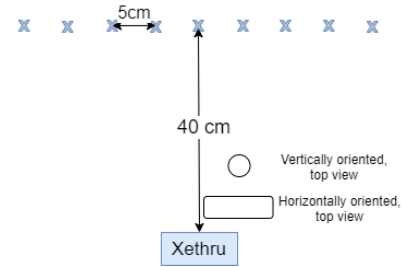**FIGURE 8.** Photo of experimental scene.

FIGURE 9. Experimental setup with positioning and orientation of the target. The XeThru x4 emits pulses of 1.5 GHz at a central frequency of 8.748 GHz, with a transmitted power in compliance with FCC regulations.
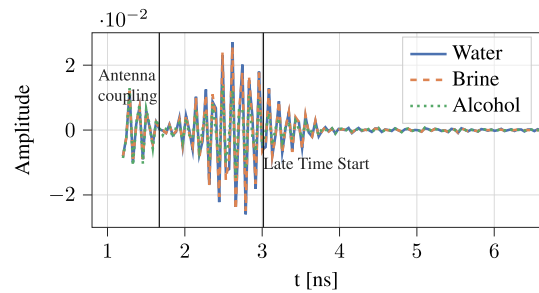

FIGURE 10. Time-domain responses for the different materials. These measurements correspond to the targets located in front of the antennas at a distance of 40 cm, horizontally aligned. The late time (Eq. (1) is considered to begin 7 samples after the first peak of the absolute value of the signal, based on the approximate time needed for the signal to travel to pass through the target and return to the antenna.

which appears to be the same across all measurements, and the beginning of the late time response. Note that for this specific scenario, the time-domain responses of the targets filled with water and brine show little difference, whereas alcohol appears to be easily distinguishable from the other two targets. However, this observation is not valid for all measurement setups because the signal amplitudes and shapes occurring from different positions and orientations vary widely for the same target, making the classification even more challenging.

To apply model (1), we discarded the early time response and retained only the late-time response. By analyzing the different captured signals, we determined that the late time began seven samples after the first peak of the absolute value of the baseband signal. This value is obtained considering the time required for the incident pulse to pass through the
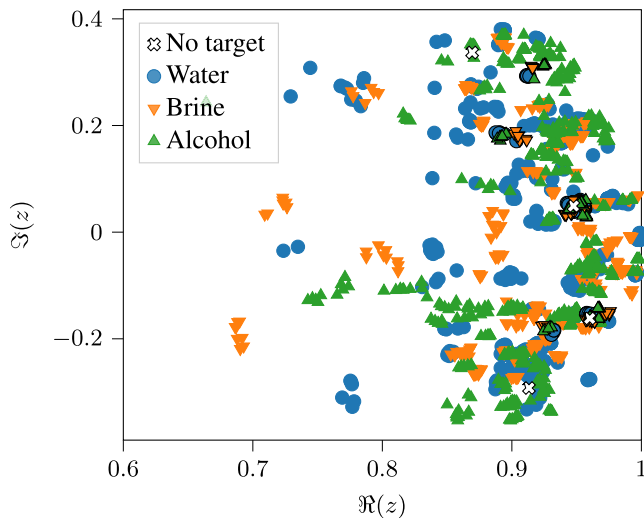
FIGURE 11. Estimated natural frequencies from the training set. Points with a black edge represent the natural frequencies discarded in the feature selection stage. Light grey crosses correspond to the resonances obtained when no target is present.

TABLE 2. Classification performance of NF and TD.

Strategy	ε	E		
			Water	Alcohol	Brine
NF	0.02	Water	95.2%	4.8%	0%
		Alcohol	1.7%	98.3%	0%
		Brine	0%	0%	100%
TD	0.34	Water	50%	32.3%	17.7%
		Alcohol	0%	89.7%	10.3%
		Brine	0%	40%	60%

target and return to the receiving antenna [41]. This method is appropriate at this stage because we assume that the target position and size are known, which is consistent with the application. However, if any of these quantities were unknown, more automatic late-time identification techniques, such as the one presented in [42], would be required.

Because nine positions for the target were considered, with two possible orientations, and 10 different samples, or measurements, were recorded for each target at each location, we had a total of 540 labeled noisy observations. These signals were split randomly into training and testing sets, 70% for training and 30% for testing.

We trained two classifiers: one using the NF approach and the other using the TD approach. For fairness, we used the same training/test splits for both approaches. For the TD strategy, we used baseband time-domain signals up to 5 ns, concatenating the real and imaginary parts as described for the synthetic data. The second classifier trained under the NF strategy used the following hyperparameters $d_{th} = 0.03$, $C = 0.95$, and a polynomial kernel of degree 2 for the SVM. These values correspond to the best solutions obtained via cross validation.

Figure 11 shows the natural frequencies extracted from the training data set. Points with black edges correspond to features discarded in the feature selection stage of the training algorithm. Grey crosses correspond to the natural frequencies discovered when no target was present, associated with the disturbance signal $d(t)$ in (8). Note that most of these are associated with discarded features.

The reported performance of the NF and TD classifiers was calculated over the test set. Table 2 summarizes the results for both classifiers. In both cases, alcohol is better classified than the other two substances. However, the overall performance of the ND classifier is two orders of magnitude better than

that of the TD classifier. Moreover, the TD classifier confused brine with alcohol in 40% of the test samples, whereas the ND classifier has a perfect score for the same test samples.

In addition, the training features of the NF method were stored in a sparse matrix because each target had natural frequencies located in a few clusters. By exploiting sparsity, we benefit from more efficient data storage, which is an additional advantage of the proposed classification strategy. We also observed a reduction in the number of features. After feature selection, only 103 clusters (206 features) were retained, whereas the time-domain approach used 117 sample points (234 features).

IV. CONCLUDING REMARKS

In this work, we presented a solution for contactless material classification that exploits the physical properties of scattered electromagnetic signals. We did this by incorporating model-based analysis into data-based learning techniques. By exploiting the physical model of scattered signals, we extracted the complex natural frequencies and used them as descriptors for each class. We then transformed the natural frequencies into characteristics suitable for the classification problem using statistical data analysis. This signal-processing step resulted in a reduction in the dimensionality of the problem, as an added benefit. Finally, machine learning techniques performed the classification. Although this work does not include advanced clutter reduction techniques, it is something that could be added in the future to improve the performance of the proposed method.

The proposed strategy was tested both with synthetic (simulated) data, as well as experimental data. For the synthetic data, we considered a challenging scenario in which all classes had similar CNRs. The effects of different perturbations on this model were analyzed, such as perturbations to the exact resonance values, perturbations to the residuals associated with each CNR in the SEM model, and additive noise in the time-domain. For all three scenarios, we showed a clear improvement using the proposed method in contrast to the typically employed approach of using time-domain signals as features to perform classification.

To validate the performance on experimental data, we considered targets that were indistinguishable by sight alone. This means that all three classes had the same shape and color, which makes the problem quite challenging because differences in the CNRs arise solely from the composition of

the material. As with the simulated signals, we observed a significant improvement in classification performance when we compared our approach with time-domain classification.

We also showed that the overall procedure was robust to multiple uncertainties that arise in the model. For instance, the procedure proposed in this paper tolerates uncertainties in the model order and variations in the residues associated with each natural resonance. Thus, our classification strategy is a suitable candidate for challenging classification problems where imperfect model information or measurement disturbances may hinder the performance of traditional classification methods.

REFERENCES

[1] W. W.-L. Lai, X. Dérobert, and P. Annan, "A review of ground penetrating radar application in civil engineering: A 30-year journey from locating and testing to imaging and diagnosis," *NDT&E Int.*, vol. 96, pp. 58–78, Jun. 2018.

[2] N. Zilberstein, J. A. Maya, and A. Altieri, "A BCS microwave imaging algorithm for object detection and shape reconstruction tested with experimental data," *Electron. Lett.*, vol. 57, no. 2, pp. 88–91, Jan. 2021.

[3] M. Persson, A. Fhager, H. D. Trefná, Y. Yu, T. McKelvey, G. Pegenius, J. E. Karlsson, and M. Elam, "Microwave-based stroke diagnosis making global prehospital thrombolytic treatment possible," *IEEE Trans. Biomed. Eng.*, vol. 61, no. 11, pp. 2806–2817, Nov. 2014.

[4] B. J. Mohammed, A. M. Abbosh, S. Mustafa, and D. Ireland, "Microwave system for head imaging," *IEEE Trans. Instrum. Meas.*, vol. 63, no. 1, pp. 117–123, Aug. 2014.

[5] J. Li, L. Liu, Z. Zeng, and F. Liu, "Advanced signal processing for vital sign extraction with applications in UWB radar detection of trapped victims in complex environments," *IEEE J. Sel. Topics Appl. Earth Observ. Remote Sens.*, vol. 7, no. 3, pp. 783–791, Mar. 2014.

[6] O. Schimmer, A. Gulck, F. Daschner, J. K. Piotrowski, and R. H. Knochel, "Noncontacting determination of moisture content in bulk materials using sub-nanosecond UWB pulses," *IEEE Trans. Microw. Theory Techn.*, vol. 53, no. 6, pp. 2107–2113, Jun. 2005.

[7] E. J. Baranoski, "Through-wall imaging: Historical perspective and future directions," *J. Franklin Inst.*, vol. 345, no. 6, pp. 556–569, Sep. 2008.

[8] F. Liang, H. Lou, Y. Zhang, H. Lv, X. Yu, Q. An, Z. Li, and J. Wang, "Through-the-wall high-dimensional imaging of human vital signs by combining multiple enhancement algorithms using portable LFMCW-MIMO radar," *Measurement*, vol. 195, May 2022, Art. no. 111074.

[9] R. Salman, T. Schultze, and I. Willms, "UWB material characterisation and object recognition with applications in fire and security," in *Proc. IEEE Int. Conf. Ultra-Wideband*, vol. 2, Sep. 2008, pp. 203–206.

[10] G. Agresti and S. Milani, "Material identification using RF sensors and convolutional neural networks," in *Proc. IEEE Int. Conf. Acoust., Speech Signal Process. (ICASSP)*, May 2019, pp. 3662–3666.

[11] R. N. Khushaba and A. J. Hill, "Radar-based materials classification using deep wavelet scattering transform: A comparison of centimeter vs. millimeter wave units," *IEEE Robot. Autom. Lett.*, vol. 7, no. 2, pp. 2016–2022, Apr. 2022.

[12] M. S. El-Mahallawy and M. Hashim, "Material classification of underground utilities from GPR images using DCT-based SVM approach," *IEEE Geosci. Remote Sens. Lett.*, vol. 10, no. 6, pp. 1542–1546, Nov. 2013.

[13] D. P. O. de Sousa Piscarreta, "Study of ultra wideband modulated Gaussian pulse and its application to nondestructive and contactless characterization of materials," Ph.D. thesis, Fac. Sci. Technol., Univ. Macau, Zhuhai, China, 2014.

[14] B. Wang, H. Song, W. Rhee, and Z. Wang, "Overview of ultra-wideband transceivers—System architectures and applications," *Tsinghua Sci. Technol.*, vol. 27, no. 3, pp. 481–494, Jun. 2022.

[15] A. Wood, R. Wood, and M. Charnley, "Through-the-wall radar detection using machine learning," *Results Appl. Math.*, vol. 7, Aug. 2020, Art. no. 100106.

[16] M. Malajner, D. Gleich, and P. Planinsic, "Material identification using UWB," in *Proc. 14th Int. Conf. Adv. Technol., Syst. Services Telecommun. (TELSIKS)*, Oct. 2019, pp. 232–234.

[17] J.-H. Lee, I.-S. Choi, and H.-T. Kim, "Natural frequency-based neural network approach to radar target recognition," *IEEE Trans. Signal Process.*, vol. 51, no. 12, pp. 3191–3197, Dec. 2003.

[18] C. E. Baum, "On the singularity expansion method for the solution of electromagnetic interaction problems," Air Force Weapons Lab., Kirkland AFB, NM, USA, EMP Interact. Note 8, 1971.

[19] T. K. Sarkar, S. Park, J. Koh, and S. M. Rao, "Application of the matrix pencil method for estimating the SEM (singularity expansion method) poles of source-free transient responses from multiple look directions," *IEEE Trans. Antennas Propag.*, vol. 48, no. 4, pp. 612–618, Apr. 2000.

[20] W. Lee, T. K. Sarkar, H. Moon, and M. Salazar-Palma, "Identification of multiple objects using their natural resonant frequencies," *IEEE Antennas Wireless Propag. Lett.*, vol. 12, pp. 54–57, 2013.

[21] W. C. Chen and N. V. Z. Shuley, "Robust target identification in white Gaussian noise using canonical correlation analysis," *IEEE Trans. Antennas Propag.*, vol. 60, no. 7, pp. 3533–3537, Jul. 2012.

[22] W. C. Chen and N. V. Z. Shuley, "Robust target identification using a modified generalized likelihood ratio test," *IEEE Trans. Antennas Propag.*, vol. 62, no. 1, pp. 264–273, Jan. 2014.

[23] J. A. Garzon-Guerrero, D. P. Ruiz, and M. C. Carrion, "Classification of geometrical targets using natural resonances and principal components analysis," *IEEE Trans. Antennas Propag.*, vol. 61, no. 9, pp. 4881–4884, Sep. 2013.

[24] M. H. Bannis, F. M. El-Hefnawi, H. M. A. El Kader, K. ElMahgoub, and A. Z. Elsherbeni, "Breast cancer detection and identification using prony's method," in *Proc. IEEE Antennas Propag. Soc. Int. Symp. (APSURSI)*, Jul. 2014, pp. 1926–1927.

[25] Y. Zaky, N. Fortino, J.-Y. Dauvignac, and B. Miramond, "Objects classification based on UWB scattered field and SEM data using machine learning algorithms," in *Proc. 18th Eur. Radar Conf. (EuRAD)*, Apr. 2022, pp. 369–372.

[26] Y. Zaky, N. Fortino, B. Miramond, and J. Dauvignac, "Generalization ability of deep learning algorithms trained using SEM data for objects classification," *Radio Sci.*, vol. 57, no. 12, pp. 1–18, Dec. 2022.

[27] M. Bouza, A. O. Altieri, and C. G. Galarza, "UWB target classification using SVM," in *Proc. IEEE Biennial Congr. Argentina (ARGENCON)*, Jun. 2018, pp. 1–8.

[28] P. Stoica and R. Moses, *Spectral Analysis of Signals*. Upper Saddle River, NJ, USA: Prentice-Hall, 2005.

[29] R. Albert and C. G. Galarza, "Model order estimation for a sum of complex exponentials," 2021, arXiv:2110.09616.

[30] F. Andersson, M. Carlsson, J.-Y. Tourneret, and H. Wendt, "A new frequency estimation method for equally and unequally spaced data," *IEEE Trans. Signal Process.*, vol. 62, no. 21, pp. 5761–5774, Nov. 2014.

[31] R. Badeau, B. David, and G. Richard, "Selecting the modeling order for the ESPRIT high resolution method: An alternative approach," in *Proc. IEEE Int. Conf. Acoust., Speech, Signal Process.*, vol. 2, May 2004, p. ii-1025.

[32] J. Papy, L. De Lathauwer, and S. Van Huffel, "A shift invariance-based order-selection technique for exponential data modelling," *IEEE Signal Process. Lett.*, vol. 14, no. 7, pp. 473–476, Jun. 2007.

[33] M. Gavish and D. L. Donoho, "Optimal shrinkage of singular values," *IEEE Trans. Inf. Theory*, vol. 63, no. 4, pp. 2137–2152, Apr. 2017.

[34] R. J. Albert and C. G. Galarza, "Model order selection for sum of complex exponentials," in *Proc. IEEE URUCON*, Nov. 2021, pp. 561–565.

[35] M. R. Anderberg, *Cluster Analysis for Applications* (Probability & Mathematical Statistics Monograph). Amsterdam, The Netherlands: Elsevier, 1973.

[36] W. H. Kruskal and W. A. Wallis, "Use of ranks in one-criterion variance analysis," *J. Amer. Stat. Assoc.*, vol. 47, no. 260, pp. 583–621, 1952.

[37] C. J. C. Burges, "A tutorial on support vector machines for pattern recognition," *Data Mining Knowl. Discovery*, vol. 2, no. 2, pp. 121–167, Jun. 1998.

[38] A. Altieri, M. Bouza, J. A. Maya, and C. G. Galarza, "Design and evaluation of an impulsive ultrawideband system for estimating the moisture content of polyamide targets," *IEEE Trans. Instrum. Meas.*, vol. 70, pp. 1–9, 2021.

[39] J. A. Garzón-Guerrero, D. Salas-González, D. P. Ruiz, and M. C. Carrión, "Neural networks and principal component analysis applied to automatic radar target recognition based on natural resonances," *Int. J. Comput. Sci. Appl.*, vol. 5, pp. 49–56, Jan. 2008.

[40] N. Andersen, K. Granhaug, and J. A. Michaelsen, S. Bagga, H. A. Hjortland, M. R. Knutsen, T. S. Lande, and D. T. Wisland, "A 118-mW pulse-based radar SoC in 55-nm CMOS for non-contact human vital signs detection," *IEEE J. Solid-State Circuits*, vol. 52, no. 12, pp. 3421–3433, Dec. 2017.

[41] W. C. Chen, "Radar target identification based on complex natural resonances," Ph.D. thesis, School Inf. Technol. Elect. Eng., Univ. Queensland, Brisbane, QLD, Australia, 2015.

[42] C. O. Hargrave, I. V. L. Clarkson, and H.-S. Lui, "Late-time estimation for resonance-based radar target identification," *IEEE Trans. Antennas Propag.*, vol. 62, no. 11, pp. 5865–5871, Nov. 2014.
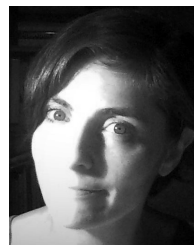
ANDRÉS ALTIERI received the Ingeniero Electrónico degree (Hons.) in electronics engineering from the University of Buenos Aires (UBA), Buenos Aires, Argentina, in 2009, and the joint Ph.D. degree from UBA and École Supérieure d'Électricité (currently CentraleSupélec), Gir-sur-Yvette, France, in 2014.

He is an Assistant Professor with the School of Engineering, UBA, and a Researcher with the National Council for Scientific and Technological Research (CONICET), Buenos Aires. He is currently a Visiting Researcher with the Laboratoire des Signaux et Systèmes, CentraleSupélec, CNRS, Université Paris-Saclay, Gif-sur-Yvette, France. His research interests include statistical signal processing and learning, microwave hardware design, and wireless sensing.

MAGDALENA BOUZA received the degree in electronic engineering from the School of Engineering, University of Buenos Aires (UBA), in 2015. In 2016, she started her Ph.D. at the University of Buenos Aires, which she is still pursuing.

She is currently an Adjunct Professor with the School of Engineering, UBA, where she is a Professor with the Specialization in Artificial Intelligence. She is currently pursuing her Ph.D., and works at DeepLearing.ai as a Curriculum Engineer.

CECILIA G. GALARZA received the degree in electronic engineering from the School of Engineering, University of Buenos Aires (UBA), in 1990, and the M.Sc. and Ph.D. degrees from the University of Michigan, Ann Arbor, in 1995 and 1999, respectively.

She is currently a Full Professor with the Faculty of Engineering, UBA, and the Director of the Center for Computational Simulations (CSC–CONICET). Her research interests include the application of signal processing to sensing and communications.

● ● ●